IRis

Northeastern University

Physics Faculty Publications

Department of Physics

May 05, 2010

Optical model-solution to the competition between a pseudogap phase and a charge-transfer-gap phase in high-temperature cuprate superconductors

Tanmoy Das
Northeastern University

R. S. Markiewicz
Northeastern University

A. Bansil
Northeastern University

Recommended Citation

Das, Tanmoy; Markiewicz, R. S.; and Bansil, A., "Optical model-solution to the competition between a pseudogap phase and a charge-transfer-gap phase in high-temperature cuprate superconductors" (2010). *Physics Faculty Publications.* Paper 409.
http://hdl.handle.net/2047/d20004186

This work is available open access, hosted by Northeastern University.

Optical model-solution to the competition between a pseudogap phase and a charge-transfer-gap phase in high-temperature cuprate superconductors

Tanmoy Das, R. S. Markiewicz, and A. Bansil
Physics Department, Northeastern University, Boston, Massachusetts 02115, USA
(Received 30 January 2010; revised manuscript received 11 April 2010; published 5 May 2010)

We present a theoretical framework for a quantitative understanding of the full doping dependence of the optical spectra of the cuprates. In accord with experimental observations, the computed spectra show how the high-energy charge-transfer (CT) gap features persist in the overdoped regime even after the midinfrared (MIR) peak originating from the pseudogap has collapsed in a quantum critical point. In this way, we reconcile the opposing tendencies of the MIR and CT peaks to shift in opposite directions in the optical spectra with increasing doping. The competition between the pseudogap and the CT gap also results in rapid loss of spectral weight in the high energy region with doping.

DOI: 10.1103/PhysRevB.81.174504 PACS number(s): 74.20.Mn, 74.25.Gz, 74.25.Jb

I. INTRODUCTION

The question of correlations has been traditionally framed in terms of a Slater picture of itinerant electrons where an insulator forms a gap via the development of a long-range magnetic order, or a Mott picture in which the metal-insulator transition is driven by a local condition of no double occupancy. Although the Slater or the Mott picture is often invoked, many materials lie in the crossover regime where the electronic states are not well described as being either fully itinerant or fully localized. Such materials are often endowed with unique and exotic properties and are of great current interest from the viewpoint of fundamental physics as well as potential for applications. The strength of electron correlations in the cuprates has been a matter of considerable debate since the discovery of these fascinating materials.[1]

Most experiments on the cuprates show that when the undoped insulating state is doped with electrons or holes the gap feature in the spectrum moves to lower energies and collapses at a quantum critical point, consistent with the notion that electron correlation effects weaken systematically with doping.[2–4] In sharp contrast, optical experiments reveal a substantially more complex picture in that doping the insulator induces a new midinfrared (MIR) feature,[5–8] which collapses with doping much as seen in other experiments, but at the same time a high-energy charge-transfer (CT) gap feature persists even into the overdoped system with its spectral weight shifting to the MIR feature with increasing doping.[9–14] In fact, the CT feature not only persists in the optical experiments, but it moves to *higher* energies with doping, suggesting that strong electron correlation effects continue to play an important role in the cuprates at all dopings. Modeling and understanding the optical spectra of the cuprates thus becomes of key importance in unravelling the routes by which the CT insulator turns itself into a superconductor, a transition that remains poorly understood.

In our one band model, the MIR gap is associated with a Slater-type gap near the Fermi level due to the presence of antiferromagnetic (AFM) order parameter.[15] The AFM gap splits the CuO_2-band into two magnetic bands which we refer to as upper and lower magnetic bands (U/LMBs). On the other hand, the CT gap is produced by correlation or fluctuation effects, involving transitions from the coherent states near the Fermi level to higher energy incoherent states which are separated by a spectral weight loss due to the high-energy kink. We make note of the difference between our present one band model with multiband treatment of the cuprates. In three band model, the LMB has strong oxygen character and the UMB is mainly copperlike, making this a CT gap as well as a magnetic gap.[16–18]

We have obtained the optical spectra within the framework of a Hubbard model where the self-energy is obtained self-consistently in an intermediate coupling scenario to account for spin and charge fluctuations via a computation of the susceptibility over the entire doping range. We emphasize that the present model involves essentially a single free parameter, a bare U chosen to reproduce the experimental CT gap at half-filling. The bare electronic dispersion is taken as that of the local density approximation (LDA) CuO_2 band (in the tight-binding form) and a screened U is then computed at various doping levels due to charge fluctuations.[19,20] In the underdoped system a pseudogap arises from a self-consistently calculated magnetic order. Our computations reproduce quantitatively the experimentally observed doping evolution of not only the shifts in the positions of the MIR and CT-gap features, but also the rapid transfer of spectral weight from the high to the low-energy region with increasing doping. The theoretical shifts of the MIR feature with doping are in accord with angle-resolved photoemission spectroscopy (ARPES)[21] and other spectroscopic probes. We emphasize that existing approaches invoking either strong or weak coupling scenarios fail to capture the essence of the doping evolution of the optical spectra.

This paper is organized as follows. In Sec. II, we compare the calculated optical spectra with experiments for both electron and hole doped cuprates. The origins of various features in the optical spectra are clarified in Sec. II A by comparison to the corresponding ARPES spectra. Sec. II B demonstrates how the CT gap and the pseudogap evolve in opposite directions with doping, showing good agreement between the present optical calculations and experiments on a wide variety of cuprates. We discuss the doping dependence of the effective number of electrons in the in-gap states and the

 ©2010 The American Physical Society

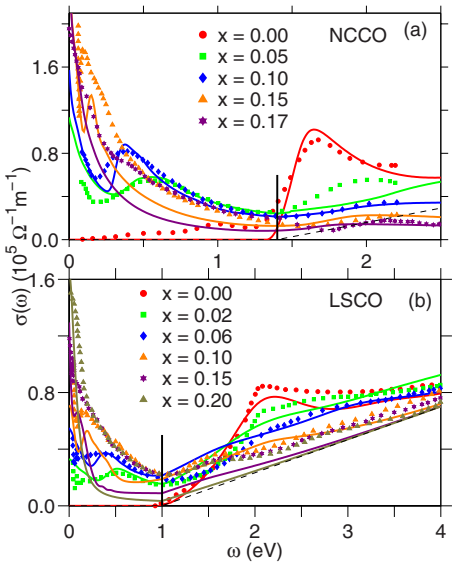

FIG. 1. (Color online) Comparison between calculated optical spectra and experiments in NCCO in (a) and LSCO in (b). Experimental results for NCCO are taken from Ref. 14, except for $x=0.17$, which, including LSCO data, are from Ref. 12. The $x=0.17$ data set for NCCO includes a background subtraction to match the former data set. Dashed line gives the background contribution added to the theoretical spectrum at $x=0$ (see Appendix B 1).

associated spectral weight transfer in Sec. III. The discussion and conclusions of our calculations are given in Sec. IV. Appendixes A and B, respectively, describe our model and the calculation of the optical conductivity.

II. OPTICAL SPECTRA IN ELECTRON AND HOLE DOPED CUPRATES

Figure 1 shows one of our key results. The computed evolution of the optical conductivity $\sigma(\omega)$ is seen to be in excellent accord with measurements on electron-doped $Nd_{2-x}Ce_xCuO_4$ (NCCO) and hole doped $La_{2-x}Sr_xCuO_4$ (LSCO).[12,14] All the spectra show a nearly isosbetic or equal absorption point near 1.3 eV for NCCO and 1 eV for LSCO [black vertical line], consistent with the experimental behavior.[23] The doping evolution is completely different on opposite sides of this isosbetic point. Above this point, the spectrum is dominated by a broad hump feature associated with the CT gap. At half-filling, only this feature is present and the calculated optical spectra show an insulating gap whose energy, structure, and intensity match remarkably with measurements.[12,14] As doping increases, the high-energy peak shifts to higher energy and broadens and its spectral weight is transferred to the Drude and MIR peaks. The MIR peak shifts to lower energy with doping and gradually sharpens. Note that in both samples at the highest doping, when the MIR peak collapses into the Drude peak, CT-gap features are still present in the spectrum. The doping evolution also shows similar behavior in other cuprates.[9–14,24] Notably, our calculations also describe the anomalous $\sigma \sim 1/\omega$-dependence found in most cuprates and associated with magnetic scattering.

A. Origin of optical dichotomy

Figure 2 helps delineate the microscopic origin of these features by comparing the spectral intensities relevant for

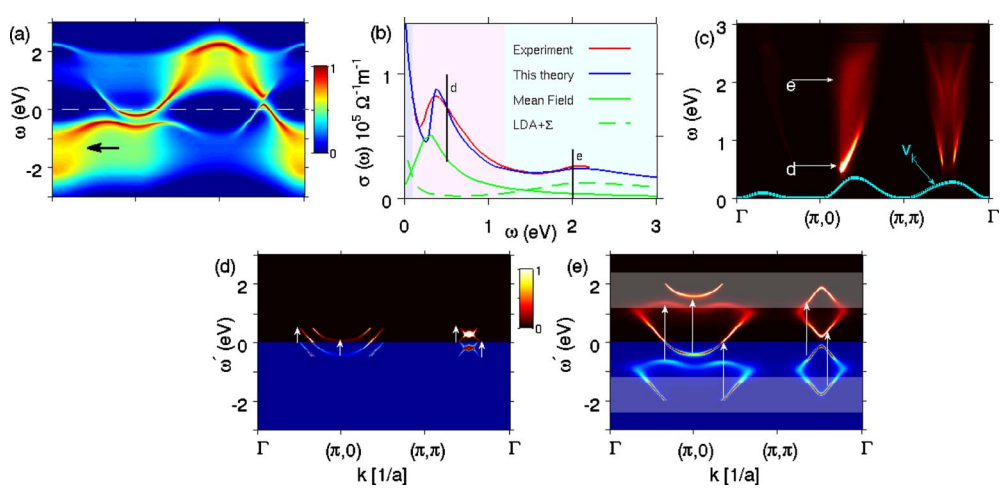

FIG. 2. (Color online) Connection between optical spectra and spectral intensity maps in NCCO. (a) Computed spectral intensity (on log scale) as a function of ω along the high symmetry lines at a representative doping of $x=0.10$. (b) Calculated optical spectra are compared with the corresponding experimental results (Ref. 14). Green solid line gives the spectrum calculated with coherent bands only, i.e., without the self-energy. Dashed green line is based on using LDA bands with self-energy correction but without the pseudogap. The shaded regions of different colors (left to right) approximately mark Drude, MIR and high energy regions. Two vertical black lines indicate the photon energies at which frames (d) and (e) are calculated. (d), (e) give source and sink maps corresponding to the optical transitions at fixed photon energy ω along the high-symmetry directions. White vertical arrows indicate the photon energy connecting source and sink points involved in a particular transition. White shaded region in (e) highlights the incoherent part of the spectral weight, not visible in (d). (c) Optical spectrum as a function of photon energy is plotted along the high symmetry lines. Cyan line gives the band velocity as a function of k (arbitrary units). The two white arrows indicate the two photon energies at which (d) and (e) are calculated.

ARPES and optical spectra at a representative doping of $x=0.10$ for NCCO; similar analysis for LSCO is not shown for brevity. In the computed ARPES spectrum in Fig. 2(a), the underlying LDA dispersion is clearly visible, but the spectral weight has split into four sub-bands, as was originally found in variational cluster calculations.[25] The highest and lowest bands are an incoherent residue of the undressed bands, which we will refer to as upper and lower CT bands. The two inner bands are coherent in-gap states split by a spin density wave induced AFM gap into upper and lower magnetic bands. The in-gap states and the high energy CT bands are separated by high-energy kinks (waterfalls) predominantly associated with magnetic excitations, as observed universally in all cuprates by ARPES,[26–28] and found in quantum Monte Carlo (QMC)[29] and variational[25] calculations.

The corresponding optical spectrum in Fig. 2(b) consists of three main regions marked by shading of different color: (1) The low-frequency Drude region for $\omega \lesssim 30$ meV; (2) The MIR region; and, (3) the high-energy CT gap region for $\omega \gtrsim 1.5$ eV. We concentrate here on the MIR and CT-gap regions, and return below to comment on the Drude region. The interband optical absorption is proportional to the joint density of states (JDOS), so that at each energy we can construct a "source map" showing the filled states, which make a strong contribution to the transition, and a "sink map" showing the contribution of the corresponding empty states. Figures 2(d) and 2(e) show the states responsible for the optical transitions along the high symmetry lines at representative photon energies of $\omega=0.5$ eV near MIR peak and $\omega=2$ eV around the high energy peak [vertical bars in Fig. 2(b)]. At $\omega=0.5$ eV, the transitions are confined within the in-gap states only, whereas at $\omega=2$ eV, the optical subbands involve predominantly the incoherent region. The depletion in the optical spectral weight near the isosbetic point in Fig. 1 and in Fig. 2(b) is thus associated with the "waterfall" region marked by arrows in the ARPES spectrum in Fig. 2(a).[23]

The total optical spectral weight obtained in Fig. 2(b) is the integral of the JDOS times the band velocity. The role of the latter factor is explicated in Fig. 2(c), where contributions to σ are plotted as a function of photon energy ω and momentum k. Although the source-sink map shows a symmetry about the $(\pi,0)$ point, the quasiparticle velocity is low along the $\Gamma \rightarrow (\pi,0)$ direction [cyan solid line in Fig. 2(c)], leading to greatly reduced spectral intensity associated with those regions. In contrast, the large quasiparticle velocity in the other two directions is responsible for two distinctive intense streaks (labeled d and e). The MIR peak is clearly dominated by the antinodal quasiparticles, whereas the high-energy hump stems from a wider k range.

B. Competition between pseudogap and CT gap

Figure 3 summarizes our results and elaborates upon the competition between the collapse of the pseudogap in the coherent bands at a critical doping, and the persistence of the CT gap in the incoherent bands. The gaps extracted from the optical spectra are now compared with other experimental data for various electron and hole-doped cuprates. The MIR gap corresponds to the true AFM gap, and its doping evolution is in good agreement with ARPES[3,15,30] and resonant inelastic x-ray scattering (RIXS)[31] results. Both ARPES and MIR data predict a QCP near $x=0.17$ (Refs. 39 and 40) consistent with the present theoretical predictions. In contrast, the CT gap shows the opposite doping dependence to the pseudogap, increasing slowly with doping. Although the CT gap does not show a real QCP, it rapidly loses intensity with doping.

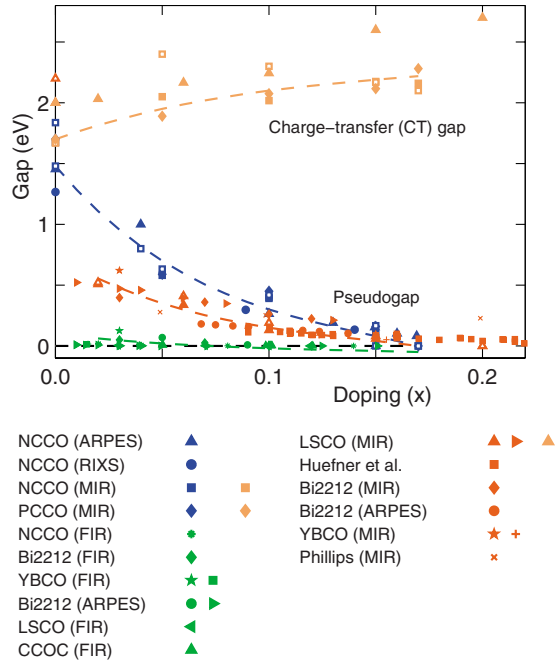

FIG. 3. (Color online) Contrasting doping dependences of the MIR and CT gaps in the cuprates. Present theoretical results are compared to optical data (Refs. 11, 12, and 14) and pseudogap data measured by ARPES (Refs. 3 and 30) and RIXS (Ref. 31) for electron doped NCCO and many other probes for hole doped cuprates. The red squares are the pseudogap for four different layered compounds (Bi2212, YBCO, TBCO, and HBCO) as obtained from ARPES, tunneling, Raman, Andreev reflection, and heat capacity experiments (reproduced from a detailed survey, Ref. 32). The second red triangles for MIR data of LSCO are taken from Lee *et al.* (Ref. 33). The red circles and '+' symbols are the pseudogap measured from ARPES on Bi2212 (Ref. 34) and optical spectra on YBCO (Ref. 35) The red "x" symbols are theoretical results (Ref. 36) for the MIR in a Mottness model ($t=0.4$ is assumed in plotting this data). The red diamond and star symbols represent independent MIR peak positions and the same symbols in green color give FIR gaps measured simultaneously in optical spectra of Bi2212 and YBCO (Ref. 37) The green circles represent a Coulomb gap seen in ARPES (Ref. 38) [energy values are obtained assuming a ratio $2\Delta/k_BT=4$]. The rest of the green symbols are reproduced from Lupi *et al.* (Ref. 37). In all cases, open symbols of same colors are our corresponding theoretical results which are obtained self-consistently at each doping. The dashed lines are guides to the eye for the CT gap (gold), the pseudogaps for electron (blue) and hole (red) doping, and the FIR and Coulomb gaps (green).

Similar results are found in hole doped LSCO,[12,33] and other layered cuprates, including $Bi_2Sr_2CaCu_2O_{8+\delta}$ (Bi2212),[10] $YBa_2Cu_3O_{6+x}$ (YBCO),[9] $Tl_2Ba_2CuO_{6+\delta}$ (TBCO),

and $HgBa_2Ca_2Cu_3O_{8+\delta}$ (HBCO)[24] as well as in x-ray absorption spectroscopy[22] and QMC computations.[41] Fig. 3 also includes data on the MIR gap for LSCO, Bi2212 and YBCO and the pseudogap obtained from a wide range of experimental data, including a recent detailed survey[32] (see Fig. 3 caption). In the intermediate and high doping regimes, there is very good agreement between the MIR and other measures of the pseudogap, while the MIR data provide important evidence for the rapid growth of the pseudogap in the deeply underdoped regime, consistent with theory. We note that while all the hole-doped cuprates seem to have a very similar doping dependence of the pseudogap, there are subtle differences with electron doped cuprates, including the steepness of the rise at low doping and the exact position of the QCP.[32,42] The former difference seems to be correlated with the doping dependence of the screened Hubbard U's, shown in Fig. 5. Since the doping dependence is mainly a screening effect,[19,20] the difference is probably due to the strong screening associated with the van-Hove singularity (VHS) on the hole-doped side.

While our present calculations reproduce the gap structures of cuprates, particularly on energy scales ≥ 100 meV, additional effects can arise at lower energies, including coupling to phonons and impurities. In particular, Lupi *et al.*[37] find in several cuprates that in addition to the MIR feature there is an additional far-infrared (FIR) peak which appears near 10% doping and shifts to higher energies at lower doping (green symbols in Fig. 3). This seems to be a disorder effect, and has a similar doping dependence to the so-called Coulomb gap seen in ARPES (green circles and diamonds) in the low-temperature region of Bi2212.[38]

The present model predicts that the MIR feature will extrapolate to the CT gap, ~ 1.8 eV in hole doped cuprates, as $x \to 0$, whereas the experimental data at lowest doping $x \sim 0.02$, have reached only about 1/3 of that value. We make several brief points on this thorny issue: (1) Looking at the actual experimental $\sigma(\omega)$, there is a substantial transfer of spectral weight between the CT peak at $x=0$ and the MIR feature at $x=0.02$, and it is an open experimental issue whether this spectral weight transfer arises via a peak shift or by the growth of a new peak at intermediate energies. This corresponds to the theoretical debate as to whether the first doped holes go into the lower magnetic band or the midgap states. (2) We find that the screening of U in hole-doped cuprates only begins to turn off when x is reduced below 0.05, Fig. 5, and in this regime results will be sensitive to details of the metal-insulator transition. (3) More generally, disorder is likely to play a large role. In particular, in LSCO, the holes get trapped by the dopant atoms at very low doping, and the screening of U is turned off at very low temperatures.[43] Note that in this doping regime the measured Drude lifetimes are quite small, Fig. 6(b). (4) Finally, for hole-doped cuprates there is likely to be an issue of competing pseudogap phases,[44] and a striped-phase is a candidate for introducing midgap states.

We emphasize that the dichotomy between the pseudogap and CT gap and the presence of the QCP are robust features of cuprates as the computations do not involve any free parametrization except the bare doping-independent value of $U=1.7$ eV at half-filling. We have computed the doping dependence of U due to the screening effects of charge fluctuations[19,20] and obtained the effective U values shown Fig. 5.

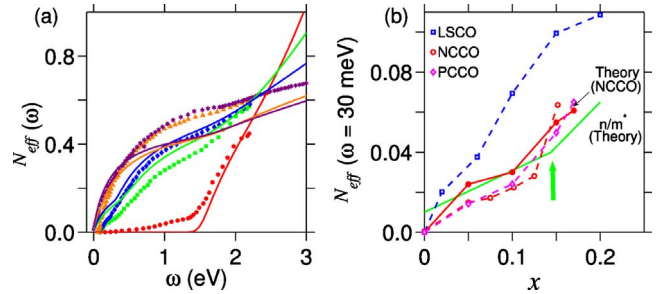

FIG. 4. (Color online) Optical sum rule and spectral weight transfer. (a) Effective number of electrons $N_{eff}(\omega)$ calculated from the optical spectra in Fig. 1 is compared with experimental data (Refs. 12 and 14) on NCCO. Results for LSCO are similar and are not shown for brevity. (b) Low-energy weight N_{eff} at $\omega=30$ meV as an estimate of Drude weight, compared with experimental results on various cuprates (Refs. 11–13). Green line gives the direct computation of the normalized Drude weight n/m^*.

III. OPTICAL SUM RULE

Finally, we use the integrated optical spectral weight to illustrate the magnetic gap collapse. The effective electron number (per Cu atom), $N_{eff}(\omega)$, can be defined in terms of the optical conductivity integrated up to an energy ω:

$$N_{eff}(\omega) = \frac{2m_0 V}{\pi e^2 \hbar N} \int_0^{\omega} \sigma(\omega')d\omega', \tag{1}$$

where m_0 and e are the free-electron mass and charge, respectively, and N is the number of Cu-atoms in a cell of volume V. The results in Fig. 4(a) show how rapidly spectral weight shifts to low energies with doping, correctly reproducing the experimental behavior as well as dynamical mean-field calculations,[1] but incompatible with strong coupling models (such as the $t-J$ or $U \to \infty$ Hubbard model) where one assumes no double occupancy of Cu sites. The present intermediate coupling model of Mott gap collapse on the other hand properly captures these spectral weight transfers as a function of doping.

Our model also predicts the Drude weight $\propto \Sigma_{\mathbf{k}} n_{\mathbf{k}}/m^*_{\mathbf{k}}$, which can be compared to an experimental estimate, taken as N_{eff} at a characteristic energy $\omega=30$ meV in Fig. 4(b) for NCCO,[13] and with results for $Pr_{2-x}Ce_xCuO_4$ (PCCO)[11] and LSCO.[12] Even here the agreement is quite good. Interestingly, at low doping the Drude weight increases almost linearly with x. Within our model, this simply reflects scaling with the area of the FS pockets in the pseudogap state. At optimal doping, the weight shows a sharp jump (green arrow) associated with the appearance of the hole pocket. This transition of the FS topology is an intrinsic feature of the model and has been found in NCCO near $x \approx 0.15$ by several experimental probes such as ARPES,[3] Hall effect,[45] and superconducting penetration depth.[39] For LSCO (blue symbols), experiments[12] show a similar linear behavior of the

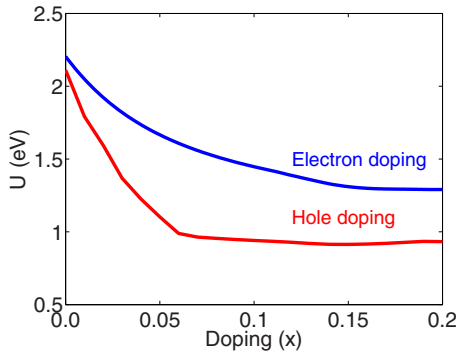

FIG. 5. (Color online) Computed screened values of U (Refs. 19 and 20) are shown for both electron and hole doped cuprates.

Drude weight, which also corresponds to the doping dependence of the area of the FS pocket.[46] The peak around $x \sim 0.2$ corresponds to the doping of the Van Hove singularity.

IV. DISCUSSION AND CONCLUSION

While a strong case can be made that in electron-doped cuprates the pseudogap is associated with a coexisting (π,π) AFM order, the nature of the pseudogap in hole doped cuprates is not well understood. There is a growing consensus that it originates from some form of density wave which acts as a competing order (which could include coupling to phonons),[47–49] and may actually also involve several competing modes, again due to proximity to the VHS.[44] However, in our earlier study of ARPES in Ref. 40, which compared several possible competing order phases, we demonstrated that the shape and doping dependence of the pseudogap in hole doping is remarkably insensitive to the particular order so long as the competing order vanishes in a QCP near optimal doping. This conclusion should hold even more strongly for the optical spectrum.

We note that recent Gutzwiller approximation (GA) +RPA calculations find a number of nesting instabilities in hole-doped cuprates, resulting in a number of competing, incommensurate density-wave orders.[44] Since the instabilities depend on the bare susceptibilities, they are located at virtually the same q-values in both the spin and charge (electron-phonon) channels. Thus, the resulting optical spectra should be very similar in both cases.

Finally, we note that our model can be used to explore the role of magnetic fluctuations as the pairing bosons for superconductivity.[50] While the study of Ref. 50 revealed a significant contribution from magnetic fluctuations, it was found that fluctuations in different frequency ranges could act cooperatively to greatly enhance T_c. This suggests that phonons could play a similar cooperative role which could explain the isotope effect.[47]

In summary, we have shown that our model framework explains the salient features of the optical spectra of cuprates and their evolution with doping at a quantitative level. The rapid loss of high energy spectral weight and the associated shift of the MIR peak to low energies in the optical spectra with increasing doping reflects collapse of the pseudogap order [here taken as a (π,π) AFM], and the presence of a QCP near optimal doping in the coherent in-gap states. By contrast, the CT gap in the incoherent states persists at all dopings including, in particular, the overdoped regime. The aforementioned coherent and incoherent states are connected via a high-energy kink driven predominately by magnetic excitations. In the magnetic excitation spectrum, the dominant excitations lie in the waterfall region, while the remnant of the low-energy magnetic resonance mode[47] is less significant.[27] Our model self-energy scheme provides a tangible basis for modeling angle-resolved photoemission,[21,51] scanning-tunnelling,[40] inelastic light scattering,[16,31] and other momentum resolved spectroscopies[52,53] of the cuprates and complex materials more generally.

ACKNOWLEDGMENTS

This work was supported by the U.S. Department of Energy, Basic Energy Sciences (Contract No. DE-FG02-07ER46352), and benefited from the allocation of supercomputer time at NERSC and Northeastern University's Advanced Scientific Computation Center (ASCC). R.S.M.'s work has been partially funded by the Marie Curie Grant (Grant No. PIIF-GA-2008-220790 SOQCS).

APPENDIX A: INTERMEDIATE COUPLING MODEL

We evaluate the self-energy Σ as a convolution over the Green function G and the interaction $W \sim U^2\chi$ as,[21,51,54,55]

$$\tilde{\Sigma}(\mathbf{k},\sigma,i\omega_n) = \frac{1}{2}U^2 Z \sum_{\mathbf{q},\sigma'}{}' \eta_{\sigma,\sigma'} \int_0^\infty \frac{d\omega_p}{2\pi}$$

$$\tilde{G}(\mathbf{k}+\mathbf{q},\sigma',i\omega_n,\omega_p)\Gamma(\mathbf{k},\mathbf{q},i\omega_n,\omega_p)\mathrm{Im}[\tilde{\chi}^{\sigma\sigma'}_{\mathrm{RPA}}(\mathbf{q},\omega_p)]. \tag{A1}$$

where σ is the spin index and the prime over the $\mathbf{q}$ summation means that the summation is restricted to the magnetic Brillouin zone. Here the spin degree of freedom $\eta_{\sigma,\sigma'}$ takes the value of 2 for the transverse direction and 1 for both longitudinal and charge modes, described below. In the underdoped region, the pseudogap is modeled by a (π,π) antiferromagnetic (AFM) order parameter, resulting in G, χ and Σ becoming 2×2 tensors.[56] The symbol "tilde" over a quantity means that it is a 2×2-tensor.

We take the dispersions directly from the LDA calculations ($\xi_{\mathbf{k}}$), accurately fitted by a one band tight-binding model,[57–61] without any adjustment of the resulting parameters. The AFM order splits the band into upper and lower magnetic bands (U/LMB): $E^{\pm}_{\mathbf{k}} = (\xi^{+}_{\mathbf{k}} \pm E_{0\mathbf{k}})$ with $\xi^{\pm}_{\mathbf{k}} = (\xi_{\mathbf{k}} \pm \xi_{\mathbf{k}+\mathbf{Q}})/2$ and $E_{0\mathbf{k}} = \sqrt{(\xi^{-}_{\mathbf{k}})^2 + (US)^2}$. Here S is the AFM order parameter evaluated self-consistently at each doping using mean-field approximation (Ref. 40). The doping dependence of the onsite Hubbard U is obtained due to charge screening from $U = \langle V(q)/(1+V(q)\chi_0^{\sigma\sigma}(q)\rangle$, where $V(q)$ is the long-range Coulomb interaction[20] and $\chi_0^{\sigma\sigma}(q)$ is the charge susceptibility in the gapped state defined below. A doping independent bare $U = 1.7$ eV is used which reproduces the

charge transfer gap at half-filling.[19,20] The obtained values of screened U are given in Fig. 5.

The Green's function in the AFM state is given by

$$\tilde{G}_{11}(\mathbf{k},\sigma,i\omega_n,\omega_p) = \alpha_{\mathbf{k}}^2 g^+(\mathbf{k},i\omega_n,\omega_p) + \beta_{\mathbf{k}}^2 g^-(\mathbf{k},i\omega_n,\omega_p)$$

$$\tilde{G}_{12}(\mathbf{k},\sigma,i\omega_n,\omega_p) = \sigma\alpha_{\mathbf{k}}\beta_{\mathbf{k}}[g^+(\mathbf{k},i\omega_n,\omega_p) + g^-(\mathbf{k},i\omega_n,\omega_p)]. \tag{A2}$$

Here

$$\alpha_{\mathbf{k}} = \sqrt{\frac{1}{2}\left(1 + \frac{\xi_{\mathbf{k}}}{E_{0\mathbf{k}}}\right)}$$

$$\beta_{\mathbf{k}} = \sqrt{\frac{1}{2}\left(1 - \frac{\xi_{\mathbf{k}}}{E_{0\mathbf{k}}}\right)} \tag{A3}$$

respectively are the weights associated with the U/LMBs. And

$$g^{\pm}(\mathbf{k},i\omega_n,\omega_p) = \frac{f(ZE_{\mathbf{k}}^{\pm})}{i\omega_n - ZE_{\mathbf{k}}^{\pm} + \omega_p} + \frac{1 - f(ZE_{\mathbf{k}}^{\pm})}{i\omega_n - ZE_{\mathbf{k}}^{\pm} - \omega_p}, \tag{A4}$$

where f is the Fermi function. The other components of the Green's function can be obtained from the symmetry transformation $\mathbf{k} \to \mathbf{k}+\mathbf{Q}$.

The dressed susceptibility in the above equation is given in terms of the 2×2 RPA susceptibility as,[56]

$$\tilde{\chi}_{\mathrm{RPA}}^{c/L}(\mathbf{q},i\omega_n) = \frac{\tilde{\chi}_0^{\sigma\sigma}(\mathbf{q},i\omega_n)}{\tilde{\mathbf{1}} \pm U\tilde{\chi}_0^{\sigma\sigma}(\mathbf{q},i\omega_n)}. \tag{A5}$$

$$\tilde{\chi}_{\mathrm{RPA}}^{T}(\mathbf{q},i\omega_n) = \frac{\tilde{\chi}_0^{\sigma\bar{\sigma}}(\mathbf{q},i\omega_n)}{\tilde{\mathbf{1}} - U\tilde{\chi}_0^{\sigma\bar{\sigma}}(\mathbf{q},i\omega_n)}. \tag{A6}$$

Here, the superscripts L, c, and T stand for longitudinal, charge and transverse RPA spin susceptibilities. In the bare susceptibilities, the superscript $(\sigma\sigma)$ refers to the combined charge plus longitudinal spin-susceptibility tensor, whereas $(\sigma\bar{\sigma})$ (with $\bar{\sigma}=-\sigma$) gives the transverse susceptibility tensor, and the $\tilde{\chi}_0^{\sigma\sigma/\sigma\bar{\sigma}}(\mathbf{q},i\omega_n)$ are bare susceptibilities;

$$\tilde{\chi}_0^{\sigma\sigma/\sigma\bar{\sigma}}(\mathbf{q},i\omega_n) = -Z^2 \sum_{\mathbf{k}}' \sum_{\nu,\nu'} \tilde{S}_{\nu,\nu'}^{\sigma\sigma/\sigma\bar{\sigma}} \frac{f(ZE_{\mathbf{k}}^{\nu}) - f(ZE_{\mathbf{k}+\mathbf{q}}^{\nu'})}{i\omega_n + ZE_{\mathbf{k}}^{\nu} - ZE_{\mathbf{k}+\mathbf{q}}^{\nu'}}. \tag{A7}$$

The coherence factors $\tilde{S}_{\nu,\nu'}^{\sigma\sigma/\sigma\bar{\sigma}}$ give the amplitude of the scattering of the quasiparticles with the charge and magnon modes of the system, respectively, and the components are

$$\tilde{S}_{\nu,\nu'}^{\sigma\sigma/\sigma\bar{\sigma}}(11) = (\alpha_{\mathbf{k}}\alpha_{\mathbf{k}+\mathbf{q}} \pm \nu\nu'\beta_{\mathbf{k}}\beta_{\mathbf{k}+\mathbf{q}})^2,$$

$$\tilde{S}_{\nu,\nu'}^{\sigma\sigma/\sigma\bar{\sigma}}(12) = -\nu(\alpha_{\mathbf{k}}\beta_{\mathbf{k}} \pm \nu\nu'\alpha_{\mathbf{k}+\mathbf{q}}\beta_{\mathbf{k}+\mathbf{q}}). \tag{A8}$$

The other coherence factors in Eq. (A8) can be derived using the translational symmetry with respect to $\mathbf{Q}$.

We define a total self-energy as $\Sigma^t = US\widetilde{\tau_1} + \Sigma$, where $\widetilde{\tau_1}$ is the Pauli matrix along the x-direction and US is the AFM gap defined below. The self-energy Σ^t contains essentially two energy scales: (i) it gives rise to the SDW with an additional renormalization of the overall quasiparticle dispersions in the low-energy region, and (ii) at higher energies it produces the incoherent features responsible for the residual CT bands. We use a modified self-consistent scheme, referred to as quasiparticle-GW (QP-GW)-scheme in which G and W are calculated from an approximate self-energy $\Sigma_0^t(\omega) = US\widetilde{\tau_1} + (1-Z^{-1})\omega\tilde{\mathbf{1}}$, where the renormalization factor Z is adjusted self-consistently to match the self-energy Σ^t at low energy.[20,27,51] The vertex correction $\Gamma(\mathbf{k},\mathbf{q},\omega,\omega_p)$ in Eq. (A1) is taken as its first order approximation (Ward's identity) as $\Gamma(\mathbf{k},\mathbf{q},\omega,\omega_p) = 1/Z$. Since the k-dependence of Σ is weak,[27] we further simplify the calculation by assuming a k-independent Σ, which we calculate at a representative point $k=(\pi/2,\pi/2)$.

APPENDIX B: OPTICAL CONDUCTIVITY

Within the framework of linear response theory, the optical conductivity is given by the Kubo formula in the limit $\mathbf{q} \to 0$

$$\sigma_{ij}(i\omega_n) = \frac{ie^2}{\omega}\sum_{\mathbf{k},\sigma}' \left\{ \mathrm{Tr}\left[\frac{n_{\mathbf{k},\sigma}}{m_{\mathbf{k},ij}}\right] - \sum_{\mathbf{k}',\sigma'}' \int_{-\infty}^{\infty} d\omega_1 \int_{-\infty}^{\infty} d\omega_2 \times \mathrm{Tr}[v_{\mathbf{k},i}A(\mathbf{k},\sigma,\omega_1)\Gamma_j^{op}(\mathbf{k},\mathbf{k}',\omega_1,\omega_2)A(\mathbf{k}',\sigma',\omega_2)] \times \frac{f(\omega_2) - f(\omega_1)}{i\omega_n + \omega_2 - \omega_1} \right\} \tag{B1}$$

where $(i,j)=x,y,z$ directions. Real frequency optical conductivity is extracted from the Matsubara results by analytic continuation $i\omega_n \to \omega + i/\tau$, where τ is the impurity scattering term, discussed below. The first term corresponds to the diamagnetic response kernel (Drude weight) which only depends on the Fermi surface topology and the second term (paramagnetic) gives the dynamical contribution to the optical response.[62] The $v_{\mathbf{k},i}$ ($m_{\mathbf{k},ij}$) are the band velocities (masses) of the coherent band and $n_{\mathbf{k},\sigma}$ is the momentum density of quasiparticles at the Fermi surface. The spectral weights $A(\mathbf{k},\omega)$ are obtained from the imaginary part of the full self-energy dressed Green function. Finally, the optical vertex correction is approximated by its lowest order term as $\Gamma_j^{op}(\mathbf{k},\mathbf{k}',\omega_1,\omega_2) \to v_{\mathbf{k},j}\delta_{\mathbf{k},\mathbf{k}'}\delta_{\sigma,\sigma'}$.

1. High-energy background

At high energies, we subtract off a linear-in-ω background from the experimental spectra associated with interband transitions to higher-lying bands not included in the present one-band calculations, consistent with supplementary Fig. 4 of Ref. 1. Figure 6(a) suggests that there may also be an extrinsic contribution to this background. We plot the results of two different optical measurements of NCCO at the same doping $x=0.10$. Both data sets show similar AFM and Mott gap magnitudes, but the older data set shows considerably

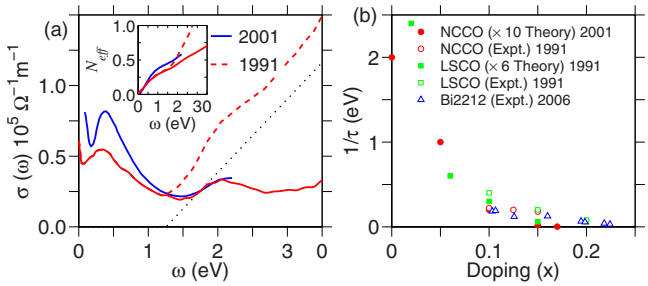

FIG. 6. (Color online) (a) Two optical spectra data taken in 2001 (Ref. 14) and 1991 (Ref. 12) are compared. The red solid line replots the older data, but with a background subtraction. The black dotted line represents the background. Inset: Integrated spectral weight for the three spectra of the main frame using same color scheme. (b) Present theoretical optical scattering rate $1/\tau$ compared with experimental results on various cuprates. Experimental values of τ are normalized to compare their doping dependence with the theory (see discussion).

larger weight at higher energies. By subtracting a linear background term from the older data set (black dotted line), it matches with the newer data very well. Remarkably, the linear term has the same form and onset as the background term used in Fig. 1. One possible origin of the larger extrinsic background of the older sample could be a problem often encountered in growing single crystals—misoriented crystallites, leading to a leaking of σ_c into the in-plane spectrum. The group of bands nearest the Fermi level are expected to be of Cu d_{z^2} or apical O p_z character, hence with enhanced c-axis conductivity, as recently noted in tunneling studies.[63]

2. Impurity effect

While keeping fixed the calculated weights of the Drude peaks, we have phenomenologically broadened the spectra with additional constant impurity scattering rates (τ). The role of impurity scattering in broadening the MIR peak can be seen by comparing the two data sets in Fig. 6(a), with the newer and presumably cleaner sample showing sharper features. It is important to note that the inset of Fig. 6(a) shows that the integrated optical spectra from both experiments are very similar in the MIR region, suggesting that impurity scattering broadens the MIR spectra but does not change the total spectral weight under the curve.[22] Figure 6(b) compares our theoretical values of $1/\tau$ with a recent experiment in Bi2212,[10] showing similar magnitude and doping dependence of the scattering in both hole-doped cuprates.

[1] A. Comanac, Luca de Medici, Massimo Capone, and A. J. Millis, Nat. Phys. **4**, 287 (2008).
[2] A. Damascelli, Zahid Hussain, and Zhi-Xun Shen, Rev. Mod. Phys. **75**, 473 (2003).
[3] N. P. Armitage, F. Ronning, D. H. Lu, C. Kim, A. Damascelli, K. M. Shen, D. L. Feng, H. Eisaki, Z.-X. Shen, P. K. Mang, N. Kaneko, M. Greven, Y. Onose, Y. Taguchi, and Y. Tokura, Phys. Rev. Lett. **88**, 257001 (2002).
[4] M. Le Tacon, A. Sacuto, A. Georges, G. Kotliar, Y. Gallais, D. Colson, and A. Forget, Nat. Phys. **2**, 537 (2006).
[5] K. Haule and G. Kotliar, EPL **77**, 27007 (2007).
[6] S. Chakraborty, Dimitrios Galanakis, and Philip Phillips, Phys. Rev. B **78**, 212504 (2008).
[7] A. S. Mishchenko, N. Nagaosa, Z.-X. Shen, G. De Filippis, V. Cataudella, T. P. Devereaux, C. Bernhard, K. W. Kim, and J. Zaanen, Phys. Rev. Lett. **100**, 166401 (2008).
[8] L. Vidmar, J. Bonca, and S. Maekawa, Phys. Rev. B **79**, 125120 (2009).
[9] S. L. Cooper, D. Reznik, A. Kotz, M. A. Karlow, R. Liu, M. V. Klein, W. C. Lee, J. Giapintzakis, D. M. Ginsberg, B. W. Veal, and A. P. Paulikas, Phys. Rev. B **47**, 8233 (1993).
[10] J. Hwang, T. Timusk, and G. D. Gu, J. Phys.: Condens. Matter **19**, 125208 (2007).
[11] T. Arima, Y. Tokura, and S. Uchida, Phys. Rev. B **48**, 6597 (1993).
[12] S. Uchida, T. Ido, H. Takagi, T. Arima, Y. Tokura, and S. Tajima, Phys. Rev. B **43**, 7942 (1991).
[13] Y. Onose, Y. Taguchi, K. Ishizaka, and Y. Tokura, Phys. Rev. Lett. **87**, 217001 (2001).
[14] Y. Onose, Y. Taguchi, K. Ishizaka, and Y. Tokura, Phys. Rev. B **69**, 024504 (2004).
[15] C. Kusko, R. S. Markiewicz, M. Lindroos, and A. Bansil, Phys. Rev. B **66**, 140513(R) (2002).
[16] R. S. Markiewicz and A. Bansil, Phys. Rev. Lett. **96**, 107005 (2006).
[17] In a one band model, this insulating gap is often treated as an effective Mott gap (Ref. 18), but we will not use this notation.
[18] F. C. Zhang and T. M. Rice, Phys. Rev. B **37**, 3759 (1988).
[19] J. Kanamori, Prog. Theor. Phys. **30**, 275 (1963).
[20] R. S. Markiewicz and A. Bansil, Phys. Rev. B **75**, 020508(R) (2007).
[21] S. Basak, T. Das, H. Lin, J. Nieminen, M. Lindroos, R. S. Markiewicz, and A. Bansil, Phys. Rev. B **80**, 214520 (2009).
[22] C. T. Chen, F. Sette, Y. Ma, M. S. Hybertsen, E. B. Stechel, W. M. C. Foulkes, M. Schluter, S.-W. Cheong, A. S. Cooper, L. W. Rupp, Jr., B. Batlogg, Y. L. Soo, Z. H. Ming, A. Krol, and Y. H. Kao, Phys. Rev. Lett. **66**, 104 (1991).
[23] Interestingly, the isosbetic point in the optical spectra associated with the "waterfall" features in ARPES occurs at lower energy in LSCO than NCCO, as does the high energy kink in ARPES spectra (Refs. 27 and 28).
[24] J. J. McGuire, M. Windt, T. Startseva, T. Timusk, D. Colson, and V. Viallet-Guillen, Phys. Rev. B **62**, 8711 (2000).
[25] C. Gröber, R. Eder, and W. Hanke, Phys. Rev. B **62**, 4336 (2000).
[26] J. Graf, G.-H. Gweon, K. McElroy, S. Y. Zhou, C. Jozwiak, E. Rotenberg, A. Bill, T. Sasagawa, H. Eisaki, S. Uchida, H. Takagi, D.-H. Lee, and A. Lanzara, Phys. Rev. Lett. **98**, 067004 (2007).
[27] R. S. Markiewicz, S. Sahrakorpi, and A. Bansil, Phys. Rev. B **76**, 174514 (2007).
[28] B. Moritz, F. Schmitt, W. Meevasana, S. Johnston, E. M. Mo-

toyama, M. Greven, D. H. Lu, C. Kim, R. T. Scalettar, Z.-X. Shen, and T. P. Devereaux, New J. Phys. **11**, 093020 (2009).
[29] A. Macridin, M. Jarrell, Thomas Maier, and D. J. Scalapino, Phys. Rev. Lett. **99**, 237001 (2007).
[30] H. Matsui, T. Takahashi, T. Sato, K. Terashima, H. Ding, T. Uefuji, and K. Yamada, Phys. Rev. B **75**, 224514 (2007).
[31] Y. W. Li, D. Qian, L. Wray, D. Hsieh, Y. Xia, Y. Kaga, T. Sasagawa, H. Takagi, R. S. Markiewicz, A. Bansil, H. Eisaki, S. Uchida, and M. Z. Hasan, Phys. Rev. B **78**, 073104 (2008).
[32] S. Hüfner, M. A. Hossain, A. Damascelli, and G. A. Sawatzky, Rep. Prog. Phys. **71**, 062501 (2008).
[33] Y. S. Lee, Kouji Segawa, Z. Q. Li, W. J. Padilla, M. Dumm, S. V. Dordevic, C. C. Homes, Yoichi Ando, and D. N. Basov, Phys. Rev. B **72**, 054529 (2005).
[34] K. Tanaka, W. S. Lee, D. H. Lu, A. Fujimori, T. Fujii, Risdiana, I. Terasaki, D. J. Scalapino, T. P. Devereaux, Z. Hussain, Z.-X. Shen, Science **314**, 1910 (2006).
[35] Yu. Li, D. Munzar, A. V. Boris, P. Yordanov, J. Chaloupka, Th. Wolf, C. T. Lin, B. Keimer, and C. Bernhard, Phys. Rev. Lett. **100**, 177004 (2008).
[36] P. Phillips, arXiv:1001.5270, Rev. Mod. Phys. (to be published).
[37] S. Lupi, D. Nicoletti, O. Limaj, L. Baldassarre, M. Ortolani, P. Calvani, S. Ono, and Y. Ando, arXiv:0905.0568, Phys. Rev. Lett. (to be published).
[38] Z.-H. Pan, P. Richard, Y.-M. Xu, M. Neupane, P. Bishay, A. V. Fedorov, H.-Q. Luo, L. Fang, H.-H. Wen, Z. Wang, and H. Ding, Phys. Rev. B **79**, 092507 (2009).
[39] Tanmoy Das, R. S. Markiewicz, and A. Bansil, Phys. Rev. Lett. **98**, 197004 (2007).
[40] Tanmoy Das, R. S. Markiewicz, and A. Bansil, Phys. Rev. B **77**, 134516 (2008).
[41] M. Jarrell, Th. Maier, M. H. Hettler, and A. N. Tahvildarzadeh, Europhys. Lett. **56**, 563 (2001).
[42] J. Tallon and J. Storey, arXiv:0908.4430 (unpublished).
[43] B. M. Andersen, P. J. Hirschfeld, A. P. Kampf, and M. Schmid, Phys. Rev. Lett. **99**, 147002 (2007); F. Coneri, S. Sanna, K. Zheng, J. Lord, and R. De Renzi, Phys. Rev. B **81**, 104507 (2010).
[44] R. S. Markiewicz, J. Lorenzana, G. Seibold, and A. Bansil, Phys. Rev. B **81**, 014509 (2010); R. S. Markiewicz, J. Lorenzana, and G. Seibold, *ibid.* **81**, 014510 (2010).
[45] T. Das, R. S. Markiewicz, and A. Bansil, Phys. Rev. B **74**, 020506(R) (2006); J. Phys. Chem. Solids **69**, 2963 (2008).
[46] T. Yoshida, X. J. Zhou, D. H. Lu, Seiki Komiya, Yoichi Ando, H. Eisaki, T. Kakeshita, S. Uchida, Z. Hussain, Z.-X. Shen, and A. Fujimori, J. Phys.: Condens. Matter **19**, 125209 (2007).
[47] Jinho Lee, K. Fujita, K. McElroy, J. A. Slezak, M. Wang, Y. Aiura, H. Bando, M. Ishikado, T. Masui, J.-X. Zhu, A. V. Balatsky, H. Eisaki, S. Uchida, and J. C. Davis, Nature (London) **442**, 546 (2006).
[48] A. Bussmann-Holder, H. Keller, A. R. Bishop, A. Simon, and K. A. Müller, J. Supercond. Novel Magn. **21**, 353 (2008).
[49] A. Macridin and M. Jarrell, Phys. Rev. B **79**, 104517 (2009).
[50] R. S. Markiewicz and A. Bansil, Phys. Rev. B **78**, 134513 (2008).
[51] R. S. Markiewicz, T. Das, S. Basak, and A. Bansil, arXiv:1002.0106, J. Electron Spectrosc. Relat. Phenom. (to be published).
[52] Y. Tanaka, Y. Sakurai, A. T. Stewart, N. Shiotani, P. E. Mijnarends, S. Kaprzyk, and A. Bansil, Phys. Rev. B **63**, 045120 (2001); S. Huotari, K. Hamalainen, S. Manninen, S. Kaprzyk, A. Bansil, W. Caliebe, T. Buslaps, V. Honkimaki, and P. Suortti, *ibid.* **62**, 7956 (2000).
[53] L. C. Smedskjaer, A. Bansil, U. Welp, Y. Fang, and K. G. Bailey, J. Phys. Chem. Solids **52**, 1541 (1991); P. E. Mijnarends, A. C. Kruseman, A. van Veen, H. Schut, and A. Bansil, J. Phys.: Condens. Matter **10**, 10383 (1998).
[54] G. Vignale and M. R. Hedayati, Phys. Rev. B **42**, 786 (1990).
[55] T. Das, Ph.D. thesis, Northeastern University, 2009.
[56] J. R. Schrieffer, X. G. Wen, and S. C. Zhang, Phys. Rev. B **39**, 11663 (1989).
[57] R. S. Markiewicz, S. Sahrakorpi, M. Lindroos, Hsin Lin, and A. Bansil, Phys. Rev. B **72**, 054519 (2005).
[58] The TB parameters are taken to be doping independent in the spirit of a rigid band picture. A more realistic treatment of the doping dependence of the electronic states (see, e.g., Refs. 59–61) was not undertaken. However, we expect the rigid band model to be a good approximation for doping away from the Cu-O planes.
[59] A. Bansil, Phys. Rev. B **20**, 4035 (1979); L. Schwartz and A. Bansil, *ibid.* **10**, 3261 (1974).
[60] S. N. Khanna, A. K. Ibrahim, S. W. McKnight, and A. Bansil, Solid State Commun. **55**, 223 (1985).
[61] H. Lin, S. Sahrakorpi, R. S. Markiewicz, and A. Bansil, Phys. Rev. Lett. **96**, 097001 (2006).
[62] P. Allen, arXiv:cond-mat/0407777 (unpublished).
[63] J. Nieminen, H. Lin, R. S. Markiewicz, and A. Bansil, Phys. Rev. Lett. **102**, 037001 (2009).